Digitally Controlled Silicon Nitride Optical Switch

Suraj Sharma*[,1], Niharika Kohli[1,2], Jonathan Brière[3], Frederic Nabki[1] and Michaël Ménard[1]
[1]Department of Electrical Engineering, Ecole de Technologie Supérieure, Montréal, QC H3C 1K3, Canada
[2]CMC Microsystems, 1111 Notre-Dame West, Montréal, QC H3C 6M8, Canada
[3]AEPONYX Inc., 33 Rue Prince #200a, Montréal, QC H3C 2M7, Canada
**suraj.sharma.1@ens.etsmtl.ca*

Abstract: We report the first 1 x 3 silicon nitride optical switch using silicon electrostatic MEMS actuator with a 4.97 dB average insertion loss over the 1530 nm to 1580 nm wavelength range.

1. Introduction

Previous silicon nitride (SiN) photonic switches relied upon thermo-optic tuning of optical components, such as Mach-Zehnder multi-mode interferometers. [1, 2]. This tuning method consumes high power in comparison to electrostatically actuated microelectromechanical systems (MEMS) based optical switching solutions. Most of the MEMS based optical switches were designed for integration with silicon (Si) based photonics [3]. While Si waveguides enable compact photonic circuits with moderate propagation loss, SiN waveguides have a wider operating wavelength range with lower propagation loss [4]. MEMS integration with SiN waveguides has been limited [5, 6] due to design challenges presented by stress related deformations of suspended silicon structures covered with cladding and waveguide materials. In this work, we demonstrate experimentally the first 1 x 3 optical switch based upon the integration of SiN waveguides with a bi-axial translational silicon-on-insulator (SOI) MEMS platform.

2. Device Design

Figure 1(a) shows a schematic of our translational MEMS switching platform in a 1 x 3 planar switching configuration. The input SiN waveguide is designed over a fixed portion of Si. The three switching waveguides are located over a suspended Si MEMS platform and fixed Si. The suspended waveguide platform can be displaced bidirectionally along the x-axis by actuating the left and right switching actuators. This enables switching in the corresponding left and right output waveguides. The support beam and the independent serpentine spring also enables unidirectional motion of the waveguide platform in the negative y-axis direction. This motion of the suspended platform enables closing of the two air gaps between suspended and fixed waveguides. Hence, we refer to this as the gap closing actuator. If only the gap closing actuator is actuated, the input waveguide is aligned to the center output waveguide. This gap closing motion can be used in the left and right switching positions as well. Each actuator works based upon the principle of electrostatic pull-in. The parallel plate actuator design enables digital actuation of the waveguide platform in the desired switching positions with minimal optical loss. Figure 1(b) shows the spring and actuator dimensions for the switching actuator. Figures 1(c) and 1(d) show the actuator gap and mechanical stopper gap dimensions for the switching and gap closing actuators, respectively. The mechanical stopper gap dimension is less than the actuator gap dimensions to prevent any electric shorts between the grounded and high voltage actuator plates upon electrostatic pull-in. The switching and gap closing actuators are designed to operate at 140 V and 62 V, respectively.

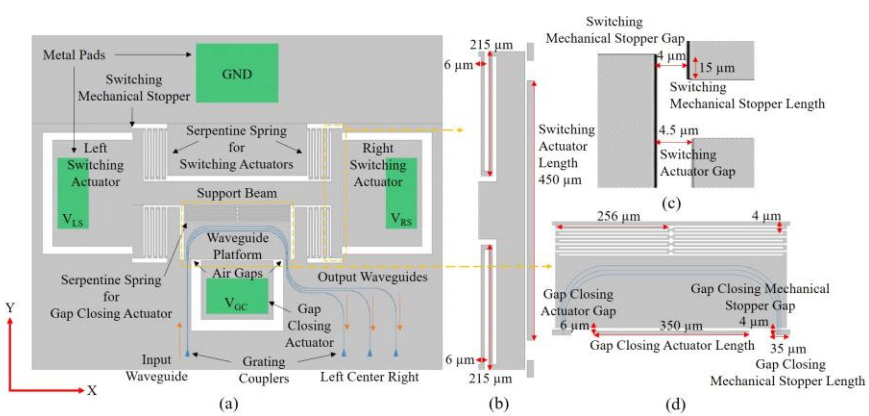

Fig. 1. (a) 1 x 3 optical switch with: (b) spring, (c) switching actuator, and (d) gap closing actuator dimensions.

3. Microfabrication and Experimental Setup

A 435 nm thick SiN waveguide layer was cladded with 3.2 µm of top and bottom silicon oxide (SiO_2). This optical stack was integrated on a silicon-on-insulator (SOI) wafer with a 59 µm thick Si device layer. The microfabrication process followed was similar to our previous work where we integrated SiN waveguides with a rotational MEMS platform [6]. Simulation results showed that a 59 µm thick device layer produces only 10 nm of stress related deformation upon integration with SiN waveguides and SiO_2 cladding. In comparison, a 10 µm device layer would result in 600 nm of deformation of the waveguide platform. The SiN waveguide cores are 450 nm wide and are surrounded by 12.3 µm of cladding on each side. Inverted tapers with a tip-width of 400 nm and a 20 µm length were included at the fixed and suspended waveguide interfaces. This was done to minimize the optical losses. The microfabrication process used requires a minimum gap of 4 µm between the fixed and suspended waveguides for successful release of the MEMS structure underneath. High resolution scanning electron microscope (SEM) images of the fabricated devices are shown in Figure 2. The mechanical stopper gap dimension came out to 4.74 µm as shown in Figure 2(b) instead of the 4 µm designed dimension presented in section 2. Similar variations in fabricated device dimensions were observed for the actuator gap. These variations increased the operational voltage for both switching and gap closing actuators. The etch profile of the optical stack is shown in Figure 2(c). This etch profile leads to a residual air gap of 1 µm between suspended and fixed SiN waveguides. The impact of these fabrication results is discussed in section 4.

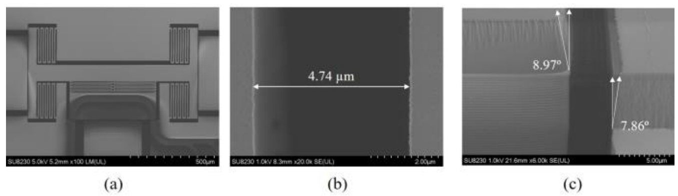

Fig. 2. (a) Fabricated 1 x 3 optical switch; (b) switching mechanical stopper gap; (c) optical stack etch profile.

The test setup used for the optical characterization of the device is shown in Figure 3(a). The fabricated device was wirebonded to a custom printed circuit board designed to control actuation during optical measurements. A tunable laser (T100S-HP) and optical component tester (CT440) from EXFO were used for these measurements. The output of the tunable laser was connected to the input of an optical fiber array with a 30º polish angle through the optical component tester. The fiber array was aligned with the surface grating couplers (SGCs) of the input and output waveguides at a vertical distance of 50 µm. Three detector ports on the optical component tester were connected to the output optical fibers from the fiber array. Polarization maintaining fibers were used to maintain the transverse electric (TE) mode during characterization. The SGCs used were optimized for the TE polarization. A microposition controller was used to align the sample to fiber array with 1 µm precision. All three switching positions were characterized with the gap closing actuator in the ON and OFF configurations to demonstrate the impact of the actuator on the optical loss. Only closing the gap actuator by applying 80 V was required for switching in the center output waveguide with minimal optical loss. The left and right switching actuators required 170 V for switching to the left and right output waveguides, respectively. The gap closing actuator was turned on in these switching positions as well to minimize optical loss. Results from these measurements are presented in section 4.

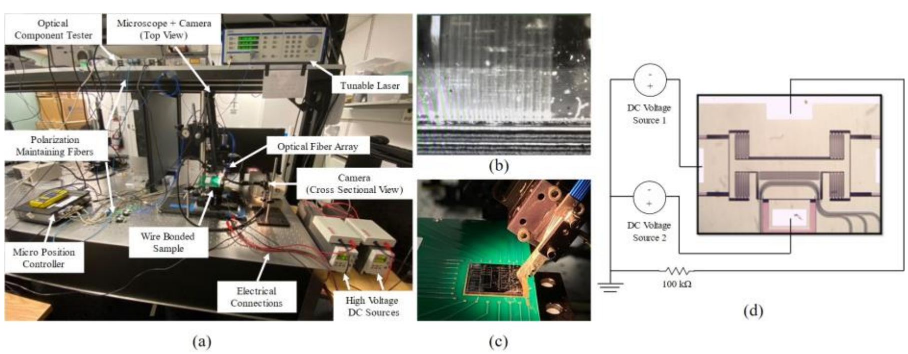

Fig. 3. (a) Optical characterization test setup; (b) optical fiber array aligned over the sample; (c) wire bonded sample during measurements; (d) test circuit used for left channel switching and gap closing actuation.

4. Results and Discussion

Figure 4(a) shows normalized transmission data for a device in three switching positions with the gap closing (GC) actuator ON and OFF. The SGCs used were optimized for a wavelength range of 1530 nm to 1580 nm. The undulations observed in the experimental results come from the SGCs. Similar undulations were observed in our reference waveguide structures. Outside the wavelength range shown, these undulations increase and require further optimization of our SGC. The average insertion loss measured over the wavelength range of 1530 nm – 1580 nm for all switching positions are shown in Figure 4(b). A minimum average insertion loss of 4.97 dB with a maximum loss reduction of 7.74 dB obtained by closing the gap was observed at the center switching position. The loss at the center position is attributed in part to the residual 1 µm distance between the suspended and fixed waveguides once the gap is closed. Moreover, the fabricated switching mechanical stopper gap of 4.74 µm vs the 4 µm originally designed causes misalignment between the suspended and fixed waveguides in the left and right switching positions, increasing insertion losses. Figure 4(c) shows the impact of the reduction in air gap between suspended and fixed waveguides at the center switching position. Measurements in Figure 4(c) were obtained at a wavelength of 1600 nm. The experimental results presented are focused on the C-band and initial L-band of the telecommunication spectrum. The waveguide configuration used in this prototype can be single mode and transparent from 1100 nm to 2200 nm with optimized SGCs.

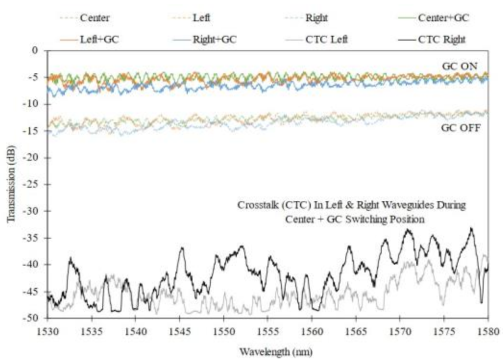

(a)

Switching Position	Average Insertion Loss (dB)
Center	12.71
Center + GC	4.97
Left	12.80
Left + GC	5.35
Right	13.52
Right + GC	6.49

(b)

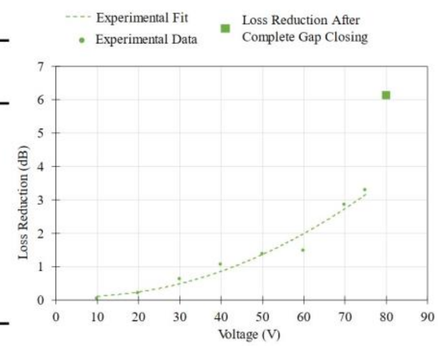

(c)

Fig. 4. (a) Transmission data in all switching positions with/without gap closing actuator across the 1530 nm – 1580 nm wavelength range; (b) average insertion loss in all switching positions; (c) optical loss reduction in the center waveguide with increase in gap closing actuator voltage.

5. Conclusion

We demonstrated the first digitally controlled SiN 1 x 3 MEMS optical switch. The novel air gap closing mechanism reduces optical losses by up to 7.74 dB providing a minimal optical loss of 4.97 dB in the center switching position. Further optimization of the optical stack etch profile can reduce losses in all switching positions. Analog (i.e., continuous) control of the switching actuator can further minimize losses and allow for an increased number of ports.

6. Acknowledgement

The authors would like to acknowledge the financial, technical and microfabrication support of AEPONYX inc. Financial support was also provided by the Natural Science and Engineering Council of Canada, PRIMA Québec and ReSMiQ.

References

[1] C. Qiu, et al., "High-Performance Graphene-on-Silicon Nitride All-Optical Switch Based on a Mach–Zehnder Interferometer," J. Light. Technol 39(7), 2099-2105 (2021).
[2] H. Nejadriahi, et al., "Thermo-optic properties of silicon-rich silicon nitride for on-chip applications," Opt. Express 28(17), 24951-24960 (2020).
[3] M. C. Wu, et al., "Large scale silicon photonics switches based on MEMS technology," in 2019 Optical Fiber Communications Conference and Exhibition (OFC), 2019, pp. 1-3.
[4] D. J. Blumenthal, et al., "Silicon nitride in silicon photonics," in Proceedings of the IEEE 106(12), 2018, pp. 2209-2231.
[5] W. Jin, et al., "Piezoelectrically tuned silicon nitride ring resonator," Opt. Express 26(3), 3174-3187 (2018).
[6] J. Briere, et al., "Rotating circular micro-platform with integrated waveguides and latching arm for reconfigurable integrated optics," Micromachines 8(12), 354 (2017).